14th International Symposium on Turbulence and Shear Flow Phenomena (TSFP14)
Heidelberg, Germany, July 28–31, 2026

THERMAL ENTRY EFFECTS IN TURBULENT PIPE FLOWS

Jonathan Neuhauser — Davide Gatti — Bettina Frohnapfel
Institute of Fluid Mechanics (ISTM)
Karlsruhe Institute of Technology
Kaiserstr. 12
jonathan.neuhauser | davide.gatti | bettina.frohnapfel@kit.edu

ABSTRACT

Well-resolved simulations of passive-scalar turbulent pipe flow in the thermal entry region are presented. We quantify thermal entry lengths of several quantities, such as the Nusselt number Nu and temperature variance, and show that they depend strongly on Re_b and Pr and that no single thermal entry length exists: higher-order statistics require much longer distances to reach their fully developed asymptote. To analyse the underlying mechanisms, we present a Nu-decomposition, the heat transfer counterpart of the Fukagata-Iwamoto-Kasagi (FIK) identity (Fukagata et al. 2002), applicable in thermally developing flow.

INTRODUCTION

Standard correlations for heat transfer in turbulent pipe flows (e.g. Gnielinski (1975)) assume axially fully developed conditions, i.e. balance between axial conduction and radial (molecular and turbulent) diffusion. In this state, mean axial fluxes of momentum and energy are constant and cancel in a cylindrical control volume aligned with the pipe axis; the flow is considered in equilibrium with the thermal boundary condition. This state is typically assumed far downstream of changes in the thermal boundary condition.

Relaxing this assumption leads to the turbulent *Graetz problem*, which considers the response of the temperature field to a step change in the thermal boundary condition (e.g. at the inlet of a heated section) while the velocity field is already hydrodynamically developed (*thermally developing flow*). The distance required for a quantity to be indistinguishable from the fully developed state is called *thermal entry length* of that quantity. Notter and Sleicher (1972), using measured turbulent velocity profiles and an eddy diffusivity model for the turbulent heat flux, reported the thermal entry length of the Nusselt number for a range of Pr and Re. They found that above a certain Pr (e.g. water, $\mathrm{Pr} \approx 7$), the entry length decreases with increasing Re (and is in the order of $5D$). In contrast, for very low Pr (e.g. liquid metals, $\mathrm{Pr} \leq 0.05$) the entry length increases significantly with Re and only saturates at a much larger distances, in the order of $30D$. This behaviour complicates experimental design and numerical studies for liquid metal heat transfer.

Well-resolved numerical studies of thermally developing internal flows are scarce; an exception is Rousta and Lessani (2022) (thermally developing channel flow, $0.71 \leq \mathrm{Pr} \leq 7$ and $\mathrm{Re}_\tau = 180$), but their domain is too short to attain fully developed first order statistics. Recently, Vicente Cruz et al. (2025) presented preliminary data on aided mixed convection in developing turbulent pipe flow. For hydrodynamic development in pipes, higher-order statistics (skewness, flatness) converge more slowly than the mean – e.g. $\sim 80D$ vs. $\sim 50D$ in Doherty et al. (2007) – implying different convergence lengths for different moments.

THEORY

We consider hydrodynamically fully developed turbulent pipe flow of a Newtonian fluid. The material properties of the fluid are assumed to be constant (in particular, independent of temperature), and temperature is modelled as a passive scalar. Viscous heating is neglected. Under these conditions, the conservation equation of temperature in cylindrical coordinates is given by Bird et al. (2007) as

$$\rho c_p \left(\frac{\partial T}{\partial t} + u_r \frac{\partial T}{\partial r} + \frac{u_\varphi}{r} \frac{\partial T}{\partial \varphi} + u_z \frac{\partial T}{\partial z} \right) = \lambda \left[\frac{1}{r} \frac{\partial}{\partial r} \left(r \frac{\partial T}{\partial r} \right) + \frac{1}{r^2} \frac{\partial^2 T}{\partial \varphi^2} + \frac{\partial^2 T}{\partial z^2} \right] \tag{1}$$

where T is the temperature, ρ, c_p, and λ are density, heat capacity at constant pressure and thermal conductivity, respectively; r, φ and z denote radial, azimuthal and axial coordinates with velocity components u_r, u_φ and u_z. For the thermal inlet problem with prescribed uniform wall heat flux q_w for $z > 0$, at the pipe's radius R, the thermal boundary conditions are

$$\lim_{z \to -\infty} T(r, \varphi, z) = T_0, \text{ for a constant } T_0, \tag{2a}$$

$$\lambda \left. \frac{\partial T}{\partial r} \right|_R = \begin{cases} q_w & \text{for } \varphi \in [0, 2\pi) \text{ and } z \geq 0, \\ 0 & \text{for } \varphi \in [0, 2\pi) \text{ and } z < 0, \end{cases} \tag{2b}$$

Various non-dimensionalisations of this problem are prevalent in the literature; they can be summarised by $u_i^* = u_i \cdot \beta / (2u_b)$, $T^* = (-1)^\delta \mathrm{Pe}^{-\gamma} 2/\beta \cdot \rho c_p (T - T_0)/q_w$, $r^* = r/(\beta R)$, $z^* = z/(\alpha \beta R)$, $t^* = t \cdot 2u_b/(\beta^2 R)$ with parameters $\beta \in \{1, 2\}$; $\gamma, \delta \in \{0, 1\}$ and α. Equations (1) and (2b) then become

$$\left(\frac{\partial T^*}{\partial t^*} + u_r^* \frac{\partial T^*}{\partial r^*} + \frac{u_\varphi^*}{r^*} \frac{\partial T^*}{\partial \varphi} + \frac{1}{\alpha} u_z^* \frac{\partial T^*}{\partial z^*} \right) = \frac{1}{\mathrm{Pe}} \left[\frac{1}{r^*} \frac{\partial}{\partial r^*} \left(r^* \frac{\partial T^*}{\partial r^*} \right) + \frac{1}{(r^*)^2} \frac{\partial^2 T^*}{\partial \varphi^2} + \frac{1}{\alpha^2} \frac{\partial^2 T^*}{\partial z^* \partial z^*} \right] \tag{3a}$$

$$\lim_{z^* \to -\infty} T^*(r^*, \varphi, z^*) = 0 \text{ for all } r^* > 0 \text{ and } \varphi \in [0, 2\pi), \tag{3b}$$

$$\left. \frac{\partial T^*}{\partial r^*} \right|_{1/\beta} = (-1)^\delta \mathrm{Pe}^{1-\gamma} \begin{cases} 1 & \text{for } \varphi \in [0, 2\pi) \text{ and } z^* \geq 0, \\ 0 & \text{for } \varphi \in [0, 2\pi) \text{ and } z^* < 0. \end{cases} \tag{3c}$$

using the Péclet number $\mathrm{Pe} = 2RU_b\rho c_p/\lambda = \mathrm{Re}_b\mathrm{Pr}$.

Denoting by $\langle a\rangle$ the statistical mean of a quantity a (obtained in practice by time averaging and averaging over the homogeneous azimuthal direction) and with a' the fluctuation $a' = a - \langle a\rangle$, the bulk temperature is defined as

$$T_b^* = \frac{\int_A \langle u_z^* T^*\rangle \mathrm{d}A}{\int_A \langle u_z^*\rangle \mathrm{d}A} = 4\beta \int_0^{1/\beta} \langle u_z^* T^*\rangle r^* \mathrm{d}r^*, \tag{4}$$

which yields the Nusselt number $\mathrm{Nu}(z)$, i.e.

$$\mathrm{Nu} = \left.\frac{\partial\langle T\rangle}{\partial r}\right|_R \frac{2R}{\langle T_w\rangle - T_b(z)} = \frac{1}{\beta}\frac{2\mathrm{Pe}^{1-\gamma}(-1)^\delta}{\langle T^*\rangle|_{1/\beta} - T_b^*(z^*)}. \tag{5}$$

In the thermally fully developed state, all statistical temperature moments are translationally invariant in z, apart from a linear increase of the mean temperature due to the constant heat input per unit length. To isolate developing effects, we subtract this linear trend by defining $\tilde{T} = -T^* + C_1\alpha z^*$, where

$$C_1 = \frac{1}{\alpha}\left.\frac{\partial\langle T^*\rangle}{\partial z^*}\right|_{z^*\to\infty} = 4(-1)^\delta \mathrm{Pe}^{-\gamma} \tag{6}$$

is known a priori from a global energy balance and represents the axial linear increase of the mean temperature in the fully developed regime. Inserting $\tilde{T}$ into eq. (3a), the mean temperature equation of $\tilde{T}$, averaged over the azimuthal direction, follows as

$$\begin{aligned} 0 &= C_1\langle u_z^*\rangle + \frac{1}{r^*}\frac{\partial}{\partial r^*}\left(\frac{r^*}{\mathrm{Pe}}\frac{\partial\langle\tilde{T}\rangle}{\partial r^*} - r^*\langle\tilde{T}'u_r^{*\prime}\rangle\right) + I_z^*, \\ \text{with} \quad \alpha I_z^* &= -\langle u_z^*\rangle\frac{\partial\langle\tilde{T}\rangle}{\partial z^*} + \frac{1}{\mathrm{Pe}}\frac{1}{\alpha}\frac{\partial^2\langle\tilde{T}\rangle}{\partial z^*\partial z^*} - \frac{\partial\langle\tilde{T}'u_z^{*\prime}\rangle}{\partial z^*} \end{aligned} \tag{7}$$

By construction, in the thermally fully developed region $\partial\langle\tilde{T}\rangle/\partial z^* = 0$, and thus $I_z^* = 0$. This follows from a global energy balance: integrating $\int_{-\infty}^{z^*}\int_0^{1/\beta}$ eq. (7)$r^*\mathrm{d}r^*\mathrm{d}z^*$ for large z^* and then differentiating with respect to z^*.

Previous studies (Kasagi et al. (2012) for channel flow, Straub et al. (2019) for pipe flow) proposed a decomposition of the global Nusselt number, suitable for thermally fully-developed conditions. This decomposition is the heat transfer analogue of the FIK skin friction decomposition by Fukagata et al. (2002), widely used in drag reduction and flow control studies. The original FIK work already treated spatially developing boundary layers, and a similar strategy is employed hereto obtain a Nu-decomposition for thermally developing flow. Evaluating $\int_{1/\beta}^0\int_{1/\beta}^r\int_{1/\beta}^{\tilde{r}}$ eq. (7)$\tilde{r}^*\mathrm{d}\tilde{r}^*\frac{1}{\bar{r}^*}\mathrm{d}\bar{r}^*\langle u_z^*\rangle r^*\mathrm{d}r^*$ yields

$$\begin{aligned} \underbrace{\frac{11}{48}}_{1/\mathrm{Nu}_{lam}} &= \frac{1}{\mathrm{Nu}} + \underbrace{(-1)^\delta\frac{\beta}{2}\mathrm{Pe}^\gamma\int_0^{1/\beta}(\Phi^*+1)\langle\tilde{T}'u_r^{*\prime}\rangle\mathrm{d}r^*}_{1/\mathrm{Nu}_{HF,r}} \\ &+ \underbrace{\frac{1}{2}\int_0^{1/\beta}\frac{\Phi_T^*}{r^*}(2\beta^4r^{*4} - 4\beta^2r^{*2} - \Phi_T^*)\mathrm{d}r^*}_{1/\mathrm{Nu}_{RSS}} \\ &\underbrace{-(-1)^\delta 2\beta^2\mathrm{Pe}^{\gamma-1}\int_0^{1/\beta}\langle u_z^{*\prime}\tilde{T}'\rangle r^*\mathrm{d}r^*}_{1/\mathrm{Nu}_{HF,z}} \\ &\underbrace{-(-1)^\delta\frac{\beta}{2}\frac{\mathrm{Pe}^\gamma}{1}\int_0^{1/\beta}\frac{\Phi^*+1}{r^*}\int_{1/\beta}^{r^*}I_z^*\tilde{r}^*\mathrm{d}\tilde{r}^*\mathrm{d}r^*}_{1/\mathrm{Nu}_{dev.}} \end{aligned} \tag{8}$$

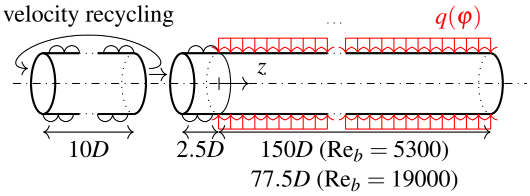

Figure 1: Sketch of the numerical setup

Re_b	L_z	nel_{cs}	nel_z	Δy_0^+	$t_{avg}u_\tau/D$
5300	150	132	702	0.29	199.7
19000	77.5	828	1152	0.26	10.5

Table 1: Metadata for the turbulent cases, including the heated streamwise length L_z, number of elements per cross section nel_{cs}, number of elements in the streamwise direction nel_z, wall distance of the first integration point and averaging time in eddy turnover times. $D = 2R$ is the pipe diameter.

where $\Phi^* = 4\beta\int_{1/\beta}^{r^*}\langle u_z^*\rangle\bar{r}^*\mathrm{d}\bar{r}^*$ is the non-dimensional fractional flow rate, so that $\Phi^*(0) = -1$. The mean axial velocity is split into a laminar and a turbulent contribution (similar to the exteded Reynolds decomposition by Gatti et al. (2018)) according to $\langle u_z^*\rangle = 1/\beta(1-\beta^2(r^*)^2) + \langle u_{z,t}^*\rangle$, and so is the fractional flow rate: $\Phi^* = \Phi_L^* + \Phi_T^* = (-1 + 2\beta^2(r^*)^2 - \beta^4(r^*)^4) + 4\beta\int_{1/\beta}^{r^*}\langle u_{z,t}^*\rangle\bar{r}^*\mathrm{d}\bar{r}^*$.

The contributions of eq. (8) are in order: a laminar part ($\mathrm{Nu}_{lam} = 48/11$ in fully developed laminar flow), Nu itself, the contribution of the radial turbulent heat flux ($\mathrm{Nu}_{HF,r}$), the modification of the bulk temperature due to the change in the mean velocity profile compared to the laminar one (Nu_{RSS}), the contribution of the axial turbulent heat flux ($\mathrm{Nu}_{HF,z}$), and a developing part (Nu_{dev}).[1] The term Nu_{RSS} is determined by the turbulent velocity profile, and, since the scalar is passive, independent of Pr. Crucially, all significant individual terms of the right-hand side of eq. (8) are observed to be positive including those originating from I_z^*; the only exceptions are the term due to the axial turbulent heat flux and the heat flux through axial conduction; the first is small (Straub et al. 2019) while the second is negligible for $\mathrm{Pe} \gg 1$. Equation (8) is reshaped as

$$1 = \frac{\mathrm{Nu}_{lam}}{\mathrm{Nu}} + \frac{\mathrm{Nu}_{lam}}{\mathrm{Nu}_{HF,r}} + \frac{\mathrm{Nu}_{lam}}{\mathrm{Nu}_{RSS}} - \frac{\mathrm{Nu}_{lam}}{\mathrm{Nu}_{HF,z}} + \frac{\mathrm{Nu}_{lam}}{\mathrm{Nu}_{dev.}}. \tag{9}$$

This decomposition can be interpreted as follows. Increasing, for example, the radial heat flux $\langle\tilde{T}'u_r^{*\prime}\rangle$ while keeping all else equal, increases $\mathrm{Nu}_{lam}/\mathrm{Nu}_{HF,r}$, which in turn must decrease the term containing Nu, i.e. $\mathrm{Nu}_{lam}/\mathrm{Nu}$, hence increasing Nu itself. This decomposition can hence be used to distinguish different mechanisms contributing to global heat transfer in the developing regime.

NUMERICAL SETUP

A turbulent flow database is created for two Reynolds ($\mathrm{Re}_b \in \{5300, 19000\}$) and Prandtl $\mathrm{Pr} \in \{0.025, 0.71\}$ numbers; the latter correspond to typical values for liquid metals and air, respectively. The governing equations are solved using the spectral element solver NekRS (Fischer et al. 2022).

[1] Note that for $I_z = 0$ (i.e. evaluated in the fully developed regime) and $\gamma = \delta = 0$, the decomposition of Straub et al. (2019) is recovered (therein, eq. (B.28) is the resulting form for $\beta = 1$ while eq. (11) is the resulting form for $\beta = 2$).

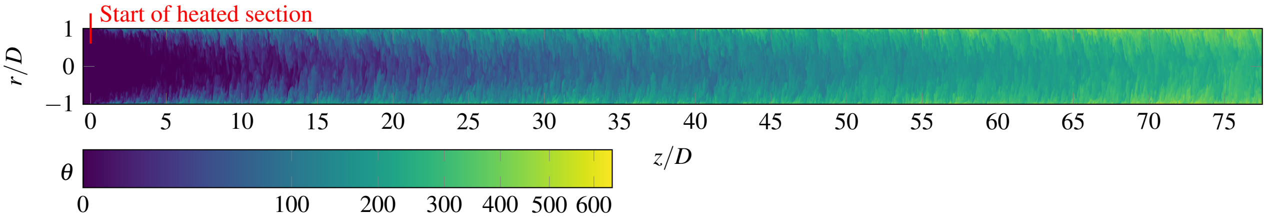

Figure 2: An r-z slice of the instantaneous dimensionless temperature for $Pr = 0.71$, $Re_b = 19000$. The horizontal axis is compressed by a factor of 5 to fit the page.

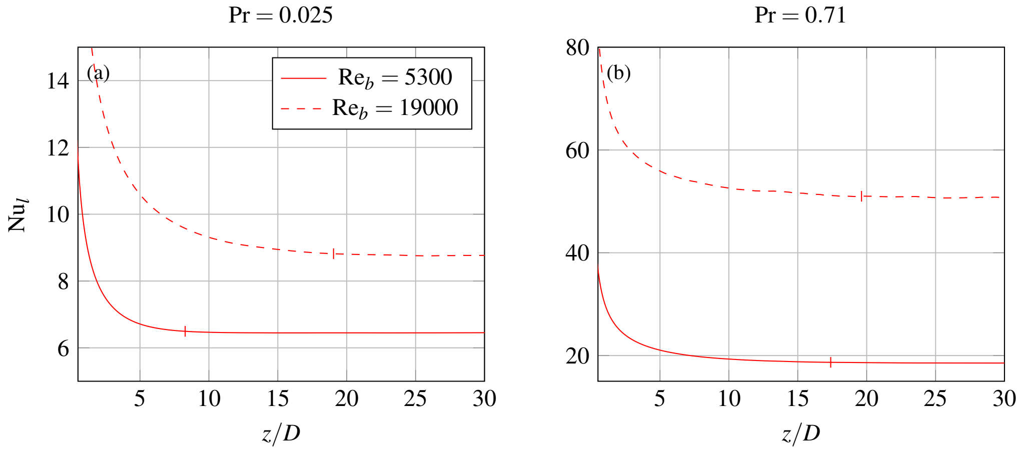

Figure 3: Azimuthal mean of the local Nusselt number as a function of z for (left) $\mathrm{Pr} = 0.025$ and (right) $\mathrm{Pr} = 0.71$ at $\mathrm{Re}_b = 5300$ (solid lines) and 19000 (dashed lines). Additionally marked is the 1% thermal entry length.

The mesh is reused from Straub et al. (2019) and extended in the axial direction, preserving axial resolution; see Straub et al. (2019) for validation. The simulation is hence a well-resolved LES for the velocity, which fully resolves the scales of temperature. BDF2/EXT2 time stepping is used, and statistics are sampled online.

A periodic precursor simulation with length $L = 10D$ is used to generate a fully developed velocity field, which is sufficient according to Pirozzoli et al. (2021). The flow in the periodic subregion has a constant flow rate. The flow then enters the heated section, which has a length of $150D$ for the $\mathrm{Re}_b = 5300$ ($\mathrm{Re}_\tau \approx 180$) case and a length of $77.5D$ for the $\mathrm{Re}_b = 19000$ ($\mathrm{Re}_\tau \approx 550$) case. This setup is illustrated in fig. 1. Metadata for the turbulent cases is given in table 1. An instantaneous visualisation of the resulting temperature field is given in fig. 2.

RESULTS
Resolved data

Figure 3 shows Nu as a function of z for both Reynolds and Prandtl numbers considered in the simulations. Its development length – defined as 1% deviation from the fully developed value – is indicated. In all cases, Nu exhibits a strong maximum at $z = 0$: At the start of the heated section, the heat flux is fixed, but the temperature profile is still nearly uniform, which results in a very high Nu. Downstream, Nu decreases monotonically towards its fully developed value; the same monotonic behaviour was found in laminar flow (Neuhauser et al. 2025).[2] For $\mathrm{Pr} = 0.025$, increasing Re_b increases the development length by a factor of 2.5; For $Pr = 0.71$, the development length only increases marginally when increasing Re_b.

Insight into the transport mechanisms in the developing region is obtained by evaluating the decomposition of Nu, using eq. (9). The resulting contributions are shown in fig. 4, in one panel for each Pe considered. Note that in all cases and for all z^*, the contributions sum up to approx. 1, verifying the decomposition eq. (9). The relevant contributions, in addition to Nu itself, are Nu_{RSS}, $\mathrm{Nu}_{HF,r}$ and $\mathrm{Nu}_{dev.}$. The term Nu_{RSS} depends only on the mean velocity profile, which is independent of z^* and determined by Re_b.

Close to $z^* = 0$, the developing term $\mathrm{Nu}_{dev.}$ dominates the balance. It consists of three parts: a positive contribution from the mean convection, a negative part from the axial turbulent heat flux (always smaller in magnitude), and a positive but extremely small part from axial conduction ($< 0.2\,\%$ even for the lowest Pe case). The ratio $\mathrm{Nu}_{lam}/\mathrm{Nu}_{dev.}$ is well approximated by an exponential decay after the temperature nonuniformity has been conducted through the viscous sublayer; this is illustrated in semi-logarithmic scaling in fig. 5. Its decay rate depends on the configuration: increasing either Re_b or Pr reduces the decay rate.

Increasing Pe (from left to right in fig. 4) enhances turbulent scalar mixing, so $\mathrm{Nu}_{HF,r}$ becomes more important. This radial heat flux contribution increases with z^*, because an increasing fraction of the turbulent eddies resides within the growing thermal boundary layer and contributes to wall-normal transport. For a given $(\mathrm{Pr}, \mathrm{Re}_b)$ configuration, the contributions corresponding to $\mathrm{Nu}_{HF,r}$, $\mathrm{Nu}_{dev.}$ and Nu approach their fully developed values with similar convergence rates.

The development length defined based on the decay of $\mathrm{Nu}_{lam}/\mathrm{Nu}_{dev.}$ agrees reasonably well with the development

[2] In buoyancy-aided flow with otherwise the same configuration, the deformation of the velocity profile near the wall is known to trigger relaminarisation at moderate Re_b, see Narasimha and Sreenivasan (1979), accompanied by a significant reduction of Nu. in the thermal entrance, this can lead to a non-monotonous behavior of Nu (Vicente Cruz et al. 2025).

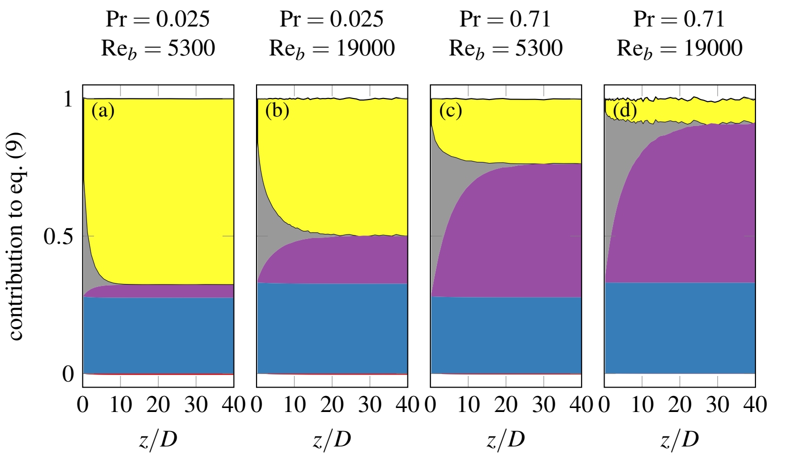

Figure 4: Individual contributions to Nu according to the decomposition eq. (9), as a function of z. Columns: $(\mathrm{Re}_b, \mathrm{Pr})$ sorted by increasing Pe from left to right. Contributions: (yellow): $\mathrm{Nu}_{lam}/\mathrm{Nu}_l$, (blue): $\mathrm{Nu}_{lam}/\mathrm{Nu}_{RSS}$, (purple): $\mathrm{Nu}_{lam}/\mathrm{Nu}_{HF,r}$, (red): $\mathrm{Nu}_{lam}/\mathrm{Nu}_{HF,z}$, (grey): $\mathrm{Nu}_{lam}/\mathrm{Nu}_{dev.}$.

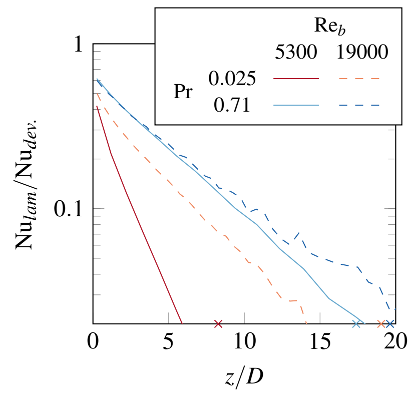

Figure 5: Contribution of the developing part to the decomposition eq. (9), i.e. $\mathrm{Nu}_{lam}/\mathrm{Nu}_{dev.}$. Additionally marked on the bottom border of the plot is the 1 % development length of Nu, see fig. 3.

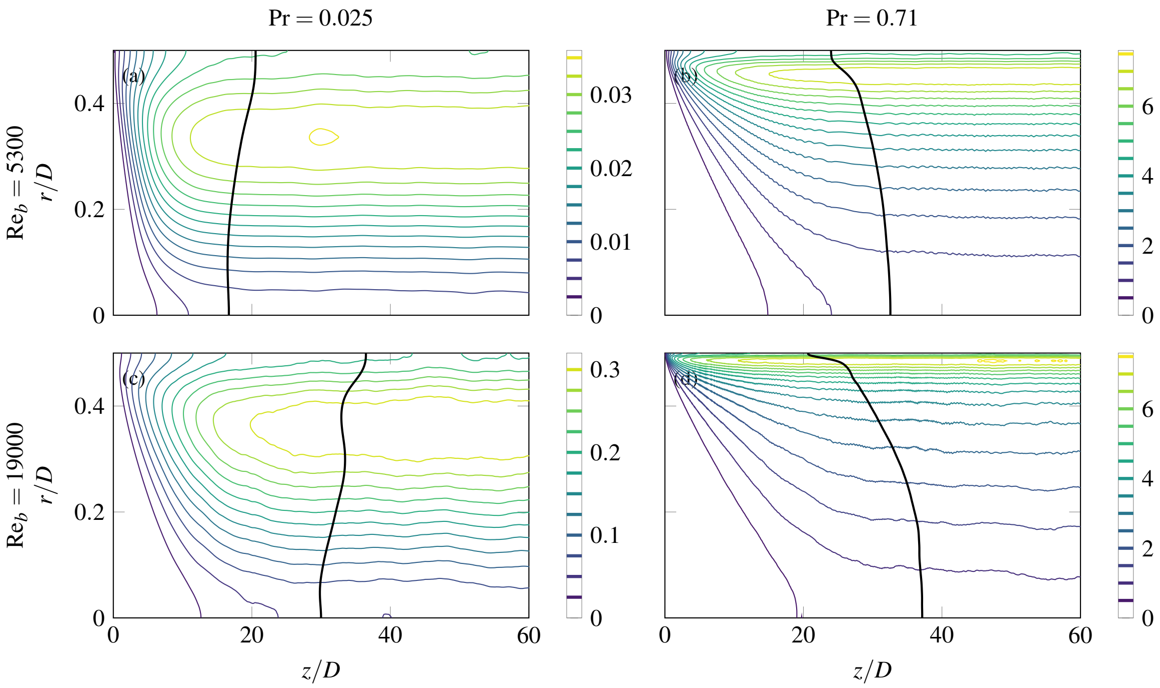

Figure 6: Contours of $\langle T^{*\prime}T^{*\prime}\rangle^+$ for uniform heat flux in the $r-z$-plane. Top row: $\mathrm{Re}_b = 5300$, bottom row: $\mathrm{Re}_b = 19000$; left column: $\mathrm{Pr} = 0.025$, right column: $\mathrm{Pr} = 0.71$. Black lines indicate the development length of this quantity, i.e. for each radial location the position where $\langle T^{*\prime}T^{*\prime}\rangle^+$ is within $0.01\,\max_r \langle T^{*\prime}T^{*\prime}\rangle^+_{z^*\to\infty}$ of the fully developed value.

length of Nu (compare lines with markers in fig. 5). Indeed the pointwise mean temperature field develops over a similar streamwise length scale as Nu.

In a turbulent temperature field, temperature fluctuations are present. Streamwise invariance of $\langle T'T'\rangle$ therefore is an indication that the *turbulent* heat transfer can be considered fully developed. From the balance equation of $\langle T^{*\prime}T^{*\prime}\rangle$, streamwise invariance of the production term

$$\mathrm{P}_{T^{*\prime}T^{*\prime}} = \langle T^{*\prime}u_r^{*\prime}\rangle \frac{\partial \langle T^*\rangle}{\partial r^*} + \langle T^{*\prime}u_z^{*\prime}\rangle \frac{\partial \langle T^*\rangle}{\partial z^*}, \qquad (10)$$

is implied when the mean temperature gradients, and thus the underlying mean temperature field, becomes invariant in the streamwise direction. One may therefore expect the development length of $\langle T^{*\prime}T^{*\prime}\rangle$ to exceed that of $\langle T^*\rangle$.

Figure 6 shows contours of the temperature variance for uniform heat flux for both Re and Pr. The thick black line in each panel marks the development length at each radius (see figure caption for the precise definition). For all configurations, the development length of $\langle T^{*\prime}T^{*\prime}\rangle$ is nearly uniform across the pipe and approx. $50-100\,\%$ higher than the corresponding development lengths of Nu and $\langle T^*\rangle$. This is in line with the *hydraulic* development behaviour of turbulent pipe flows (Doherty et al. 2007).

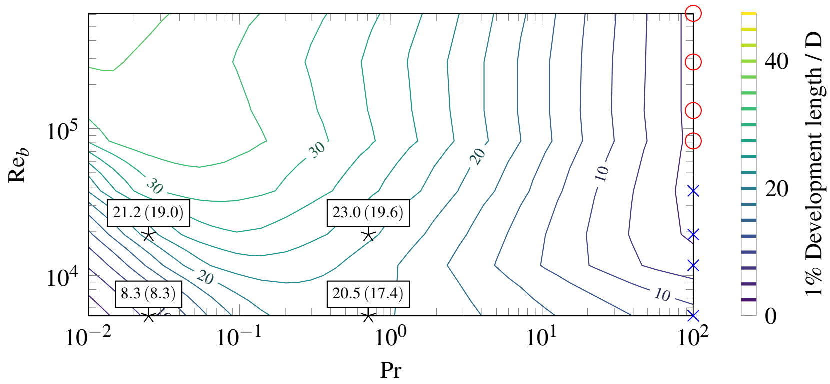

Figure 7: 1 % development length of Nu as a function of Pr and Re_b, based on the Kays correlation and DNS data for the momentum variables. On the right, markers indicate Re_b values at which DNS data was used: × (Straub 2019) for $\mathrm{Re}_b = \{5300, 11700, 19000, 37700\}$; ○ (Pirozzoli 2024) for $\mathrm{Re}_b = \{82500, 133000, 285000, 612000\}$. Points marked with ⋆ represent present (resolved) data. The label above each of those points contain the value predicted by the simplified model, and (in parentheses) the value as computed from the resolved data.

Expansion of the parameter range

For laminar flow, we showed in our paper on the *laminar* thermal entrance (Neuhauser et al. 2025), that the thermal entry length of Nu (and of all other quantities) scales with $\mathrm{Pe} = \mathrm{Re}_b\mathrm{Pr}$ for $\mathrm{Pe} \gg 1$. For turbulent flow, fig. 3 illustrated that the behaviour is more complex: for $\mathrm{Pr} = 0.025$ an increase in Re_b leads to a longer development length, whereas for $\mathrm{Pr} = 0.71$ it is almost unchanged. In the following, the parameter space in $(\mathrm{Re}_b, \mathrm{Pr})$ is explored using a gradient-diffusion closure together with DNS data for the turbulent velocity profile and eddy viscosity.

The gradient-diffusion hypothesis (Pope 2000) in dimensionless form reads

$$\langle u_r^{*\prime} T^{*\prime} \rangle = -\frac{1}{\mathrm{Pe}} \alpha_{t,r}^* \frac{\partial \langle T^* \rangle}{\partial r^*}, \qquad \langle u_z^{*\prime} T^{*\prime} \rangle = -\frac{1}{\mathrm{Pe}} \frac{\alpha_{t,z}^*}{\alpha} \frac{\partial \langle T^* \rangle}{\partial z^*}, \tag{11}$$

where $\alpha_{t,r}^*$ and $\alpha_{t,z}^*$ are the turbulent thermal diffusivities in radial and axial direction, non-dimensionalized with $\lambda/(\rho c_p)$. These are inserted into $1/(2\pi)\int_0^{2\pi} \langle \text{eq. (3a)} \rangle \mathrm{d}\varphi$:

$$\frac{\mathrm{Pe}}{\alpha} \langle u_z^* \rangle \frac{\partial \langle T^* \rangle}{\partial z^*} = \frac{1}{r^*} \frac{\partial}{\partial r^*} \left(r^* (1 + \alpha_{t,r}^*) \frac{\partial \langle T^* \rangle}{\partial r^*} \right) + \frac{\partial}{\partial z^*} \left((1 + \alpha_{t,z}^*) \frac{\partial \langle T^* \rangle}{\partial z^*} \right). \tag{12}$$

The turbulent thermal diffusivity is now approximated as isotropic and determined by the mean momentum equation (i.e. independent of z), hence one models

$$\alpha_{t,r}^* = \alpha_{t,z}^* = \alpha_{tot}^*(r) - 1. \tag{13}$$

The temperature equation then becomes

$$\langle u_z^* \rangle \frac{\partial \langle T^* \rangle}{\partial z^*} = \frac{1}{r^*} \frac{\partial}{\partial r^*} \left(\alpha_{tot}^* r^* \frac{\partial \langle T^* \rangle}{\partial r^*} \right) + \alpha_{tot}^* \frac{1}{\mathrm{Pe}^2} \frac{\partial^2 \langle T^* \rangle}{\partial z^* \partial z^*}. \tag{14}$$

The governing equation for the laminar extended Graetz problem (Papoutsakis et al. 1980) is obtained with $\alpha_{tot}^* = 1$. To close the model, the correlation of Kays (1994) is employed, i.e.

$$\alpha_{tot}^* = 1 + \frac{\mathrm{Pr}}{\mathrm{Pr}_t} \nu_t^* \quad \text{where } \mathrm{Pr}_t = 0.85 + \frac{0.7}{\mathrm{Pr}\nu_t^*} \tag{15}$$

where $\nu_t^* = \nu_t/\nu$, and ν_t is the turbulent eddy viscosity, here defined via the Boussinesq approximation $\langle u_r' u_z' \rangle = -\nu_t\, \partial \langle u_z \rangle / \partial r$.

Together with the boundary conditions eqs. (3b) and (3c), this equation can be solved numerically using $\langle u_z^* \rangle$ and ν_t^* from DNS. Data from Straub (2019) and Pirozzoli (2024) is used; the highest Re_b considered is 612 000. A second-order finite-difference discretisation is employed with suitably chosen domain length and grid resolution, and the resulting linear system is inverted directly. From the computed scalar fields, $\mathrm{Nu}(z)$ is evaluated and its development length determined. The results are shown in fig. 7.

Also indicated in fig. 7 are the points where well-resolved scalar data is available, i.e. $\mathrm{Pr} = \{0.025, 0.71\}$ and $\mathrm{Re}_b = \{5300, 19000\}$. Labels at these locations give the development length predicted by the simplified model, and in parentheses the value obtained from the resolved data. The predictions agree within about 15 %, indicating that the simplified model captures the main trends in development length.

The dependence of the development length on Re_b is strongly influenced by Pr. For low $\mathrm{Pr} \ll 1$, the development length increases with Re_b (from about $5D$ to about $35D$), whereas for high $\mathrm{Pr} \gg 1$ it decreases with Re_b (from approx. $10D$ to $5D$). For intermediate $\mathrm{Pr} \approx 0.7-10$, the development length is weakly affected by Re_b and is of the order $20D$. These trends are consistent with the results of Notter and Sleicher (1972), who used a different turbulent heat flux model and synthetic velocity profiles based on measurements.

These findings are explained as follows. Increasing Re_b has two competing effects on the development length. First, the mean convective time scale decreases (advection is faster), so for a given amount of diffusion (molecular and turbulent), a *longer* streamwise distance is needed to reach equilibrium. Second, increasing Re_b increases turbulent mixing, which enhances turbulent diffusion and thus tends to *shorten* the development length. For low Pr, turbulent diffusion contributes less to radial transport, so the first effect dominates and the development length increases with Re_b. For high Pr, turbulent diffusion dominates and the second effect prevails. At a sufficiently high Re_b, an approximate balance between both mechanisms appears at all Pr: further increasing Re_b leaves the development length almost unchanged. For example, at $\mathrm{Pr} = 100$ the development length is nearly constant for $\mathrm{Re}_b > 19000$, whereas for $\mathrm{Pr} = 0.1$ this plateau is only reached for $\mathrm{Re}_b > 10^5$.

CONCLUSION

In the thermal development region of hydraulically fully developed pipe flow subject to azimuthally uniform heat flux, the development of various quantities is examined to evaluate the onset of the fully developed state and the heat transfer mechanisms in the non-equilibrium region. This is done by expanding the Nusselt number decomposition of Straub et al. (2019) to account for thermal entrance effect, and applying it to well-resolved turbulent numerical data at $\mathrm{Pr} \in \{0.025, 0.71\}$ and $\mathrm{Re}_b = \{5300, 19000\}$.

Using convergence of the global Nu alone as criterion for the fully developed state is shown to be misleading when higher-order statistics, such as temperature fluctuations, are of interest. In laminar flow, the dependence of the development length of various quantities on Re_b and Pr is simple: for $\mathrm{Pe} \gg 1$, it scales linearly with Pe. For turbulent flow, a reduced-order model based on the gradient-diffusion hypothesis and DNS velocity profiles reveals a more complex behaviour. At fixed Pr, the development length becomes nearly constant for sufficiently high Re_b, but this value is approached from above for high Pr and from below for low Pr, with low-Pr fluids featuring much longer development lengths.

Acknowledgements We greatly acknowledge the support by the German Research Foundation (DFG) under research project 423710075. The simulations were performed on the national supercomputer HPE Cray EX4000 Hunter at the High Performance Computing Center Stuttgart (HLRS) under the grant number ctbctpf.

Author contributions (CRediT) JN: Conceptualization, Methodology, Software, Validation, Formal analysis, Investigation, Data curation, Writing, Visualization; DG: Methodology, Resources, Writing – Review & Editing, Supervision; BF: Resources, Writing – Review & Editing, Supervision, Funding acquisition

Data availability Data is available upon request.

REFERENCES

Bird, R. B., Stewart, W. E., and Lightfoot, E. N. 2007. *Transport Phenomena*. Revised second edition. New York: John Wiley & Sons, Inc.

Doherty, J., Ngan, P., Monty, J., and Chong, M. 2007. The Development of Turbulent Pipe Flow. *Australasian Fluid Mechanics Conference*. Crown Plaza, Gold Coast, Australia.

Fischer, P., Kerkemeier, S., Min, M., Lan, Y.-H., Phillips, M., Rathnayake, T., Merzari, E., Tomboulides, A., Karakus, A., Chalmers, N., and Warburton, T. 2022. NekRS, a GPU-accelerated Spectral Element Navier–Stokes Solver. *Parallel Computing* **114**, p. 102982.

Fukagata, K., Iwamoto, K., and Kasagi, N. 2002. Contribution of Reynolds Stress Distribution to the Skin Friction in Wall-Bounded Flows. *Physics of Fluids* **14.11**, pp. L73–L76.

Gatti, D., Cimarelli, A., Hasegawa, Y., Frohnapfel, B., and Quadrio, M. 2018. Global Energy Fluxes in Turbulent Channels with Flow Control. *Journal of Fluid Mechanics* **857**, pp. 345–373.

Gnielinski, V. 1975. Neue Gleichungen für den Wärme- und den Stoffübergang in turbulent durchströmten Rohren und Kanälen. *Forschung im Ingenieurwesen A*.

Kasagi, N., Hasegawa, Y., Fukagata, K., and Iwamoto, K. 2012. Control of Turbulent Transport: Less Friction and More Heat Transfer. *Journal of Heat Transfer* **134.3**, p. 031009.

Kays, W. M. 1994. Turbulent Prandtl Number—Where Are We? *Journal of Heat Transfer* **116.2**, pp. 284–295.

Narasimha, R. and Sreenivasan, K. 1979. Relaminarization of Fluid Flows. *Advances in Applied Mechanics*. Vol. 19. Elsevier, pp. 221–309.

Neuhauser, J., Metsch, J.-H., Gatti, D., and Frohnapfel, B. 2025. Solution of the Extended Graetz Problem for Nonuniform Heat Flux. *International Journal of Heat and Mass Transfer* **249**, p. 127198.

Notter, R. H. and Sleicher, C. A. 1972. A Solution to the Turbulent Graetz Problem—III Fully Developed and Entry Region Heat Transfer Rates. *Chemical Engineering Science* **27.11**, pp. 2073–2093.

Papoutsakis, E., Ramkrishna, D., and Lim, H. C. 1980. The Extended Graetz Problem with Prescribed Wall Flux. *AIChE Journal* **26.5**, pp. 779–787.

Pirozzoli, S. 2024. On the Streamwise Velocity Variance in the Near-Wall Region of Turbulent Flows. *Journal of Fluid Mechanics* **989**, A5.

Pirozzoli, S., Romero, J., Fatica, M., Verzicco, R., and Orlandi, P. 2021. One-Point Statistics for Turbulent Pipe Flow up to $\mathrm{Re}_\tau \approx 6000$. *Journal of Fluid Mechanics* **926**, A28.

Pope, S. B. 2000. *Turbulent Flows*. Cambridge ; New York: Cambridge University Press. 771 pp.

Rousta, F. and Lessani, B. 2022. Numerical Study of Thermally Developing Turbulent Internal Flows. *International Journal of Heat and Mass Transfer* **188**, p. 122623.

Straub, S. 2019. *Statistics on Turbulent Forced Convection Pipe Flow with Different Thermal Boundary Conditions for Two Prandtl Numbers*. KITopen.

Straub, S., Forooghi, P., Marocco, L., Wetzel, T., Vinuesa, R., Schlatter, P., and Frohnapfel, B. 2019. The Influence of Thermal Boundary Conditions on Turbulent Forced Convection Pipe Flow at Two Prandtl Numbers. *International Journal of Heat and Mass Transfer* **144**, p. 118601.

Vicente Cruz, R., Flageul, C., Lamballais, É., Uribe, J. C., Duffal, V., Le Coupanec, E., and Benhamadouche, S. 2025. High-Fidelity Simulation of Developing Mixed Convection in a Bouyancy-Aided Vertical Pipe Flow. *Turbulence, Heat and Mass Transfer*. Tokyo.